EUROPEAN COMMISSION

Community Research

Contract no.: 248231

MOSARIM

SIMULATION OF EFFECTS AND IMPACT OF ENVIRONMENT, TRAFFIC PARTICIPANTS AND INFRASTRUCTURE

Report type	Deliverable
Work Group	WP2
Dissemination level	Public
Version number	Version 1.1
Date	2012-08-24
Lead Partner	Karlsruhe Institute of Technology

Project Coordinator

Dr. Martin Kunert
Robert Bosch GmbH
Daimlerstrasse 6

71229 Leonberg
Phone +49 (0)711 811 37468
martin.kunert2@de.bosch.com

MOSARIM

SEVENTH FRAMEWORK PROGRAMME

Authors

Name	Company
Tom Schipper	Karlsruhe Institute of Technology

Revision chart and history log

Version	Date	Reason
0.1	2011-11-12	Initial version
0.4	2012-04-04	Basic considerations / equations added
0.5	2012-15-04	Tunnel measurements / simulations added
0.6	2012-12-05	Shielding simulations added
0.61	2012-22-06	Traffic simulations added
0.8	2012-24-06	Conclusions added
0.992	2012-08-07	Peer Review by John/Kunert
0.999	2012-09-07	Update by Schipper with respect to last peer reviews (including last review by Hildering)
V1.0	2012-13-07	Final version
V1.1	2012-24-08	Final version, revised pictures

Table of contents

Executive Summary

The influence and impact of environmental objects on interference for the single entry case is investigated in this document by means of models and simulations.

Environments with an energy-focusing characteristic like street canyons or tunnels can lead to an increased received interference power level in comparison to normal free-space / two-path propagation. Typically the maximum interference levels are occurring in near vicinity, where the two-path propagation model and antenna patterns can describe the wave propagation
If direct line-of-sight interference is present, this is dominating compared to reflections or other propagation ways. This is caused by the fact that each reflection or diffraction attenuates the signal power by several dBs and thus decreases the importance and weight of backscattered signals.
Wide antenna beams of sideward/backward/forward looking radars are increasing the received interference power levels, e.g. for applications like LCA or BSD. However, ACC has reduced interference risk due to the smaller beam width and consequently lower probability to cross another ACC radar main beam.
Basic equations are derived in this document to clarify some generic interference effects. These equations can be used to estimate the worst-case impact of a single interfering device. Eq. 3-7 especially helps to derive possible worst-case scenarios while designing practical road tests.

1. INTRODUCTION

The environment (urban, suburban, rural), infrastructure (traffic signs, road types, guardrails etc.) and traffic participants (vehicles, pedestrians) have an influence on the received interference power due to different scatter- and shielding effects. In [D22] rudimentary simulation models have been developed, and in [D24] validation checks of this simulation have been carried out.

Now this deliverable will check the influence of the environment on the expected maximum received interference power levels. Further it examines whether the scenarios, as defined in deliverable D1.2 [D12] of the MOSARIM project, "*Specification of relevant scenarios, applications and traffic conditions*", are representing significant (*or valid*) worst-case conditions. This document has the following content:

Chapter two gives a short overview of the actual status of the simulator, as well as an outlook on it's required features, which will allow more general statements about the actual and future interference situation on the road.

Chapter three introduces the basic interference mechanisms and related assertions. These are justified by practical measurements. These basics are needed to derive the influence of a disturbing waveform to the radar's relevant input signal in the frequency domain.

Chapter four presents the wave propagation tool with respect to it's capability to create multipath and shielding effects.

Chapter five describes the influence of the environment/vehicles/infrastructure
A typical road scenario is increased in complexity and the observed changes are documented and interpreted. Finally it concludes with an outlook to deliverable D2.6.

2. Overview of the current simulation chain

The simulation chain consists of three main tools, a Ray-Tracing Tool (RTT), a Scenario Editing Tool (SET) and a Simulation Flow Control Software (SFCS).

The structure of the simulation chain and its interfaces is shown in Fig. 2-1 (status as of June 2012), whereby the *statistical scenario editing* plays the key role in deliverable D2.6, "*Multi-interference modeling and effects*", which is still in a development stage.
However, the simulation chain already offers a good flexibility to investigate automotive radar scenarios.

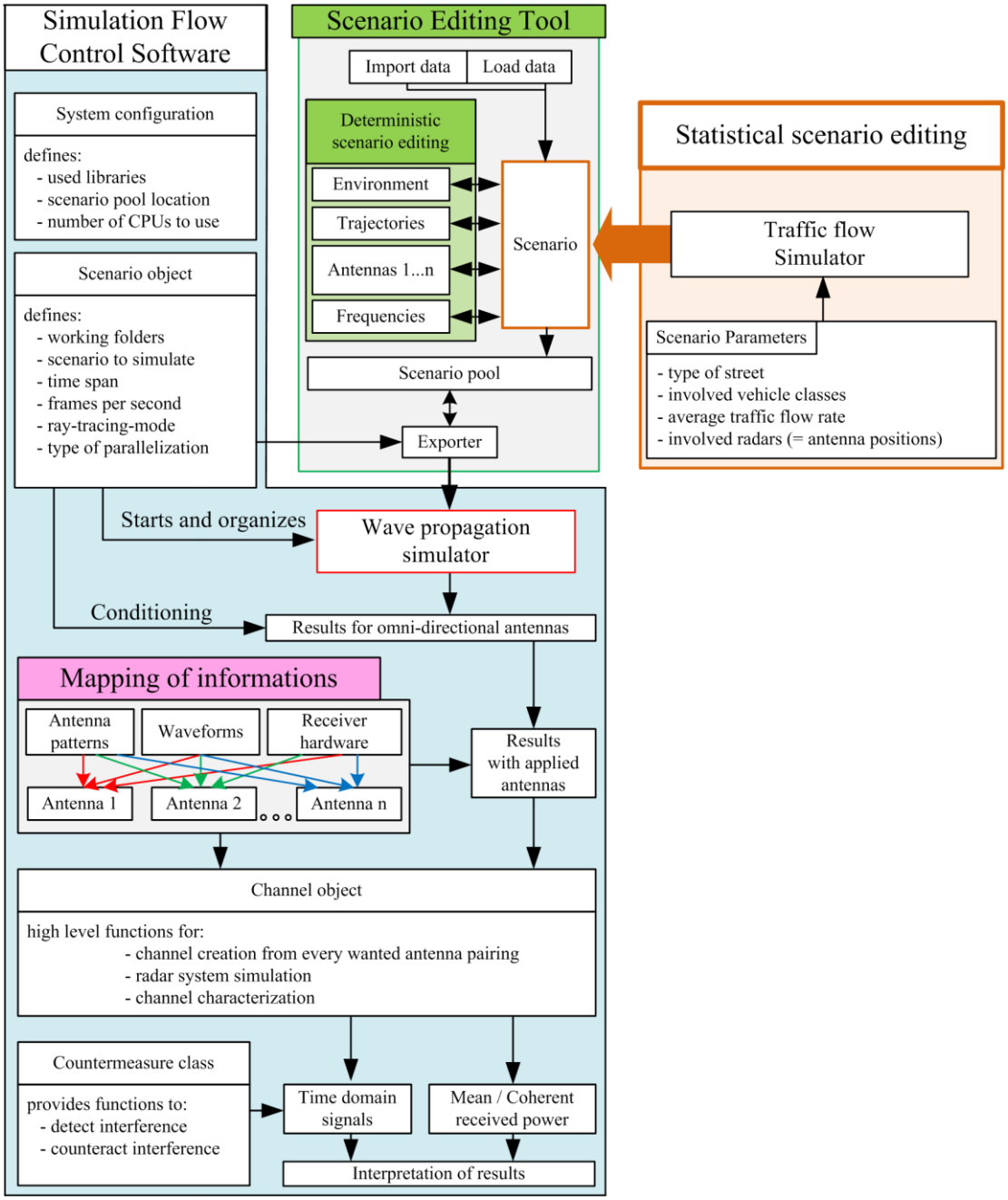

Fig. 2-1: Overview of the actual simulation approach and its interfaces

The following higher-level models have been realized, developed from the first ideas and simulation models as presented in deliverable D2.2, "Generation of an interference susceptibility model for the different radar principles"

- Fully numeric model (M1 in deliverable D2.2):

  Time-step by time-step simulation (with signal voltage values), including all hardware components and wave propagation effects for all victim radars /disturbing radars in a unique scenario. This model was first used to achieve the results already presented in deliverable D2.4.

- Mixed model (M4 in deliverable D2.2):

  Link budget calculation, based on rudimentary component data for all victim radars & disturbing radars, wave propagation simulation, and considering interference effects on an abstracted level.

  To realize a detailed (extended) scenario, a combined simulation with M1 and M4 is well suited. The wave propagation simulation has to be done (just once) only for one time, after that a fast M4 simulation allows to scan the whole scenarios for most important moments in time. These moments can then be simulated in detail with M1.

3. Basic considerations for interference into FM radar receivers

In previous MOSARIM tasks basic interference effects have already been analytically considered. For the complete simulation tool-chain they are here further developed for the most common case of frequency modulated radar systems.

3.1. Gain in signal level versus interference for FM-signals

The following Fig.3-1 is showing a FM local oscillator frequency ramp A of a radar transmitting stage. Another signal B, in this case a CW interferer signal, is crossing the signal A in the frequency over time plot. The blue lines in the areas C1 and C2 mark the resulting mixer output frequencies relative to the frequency ramp A.

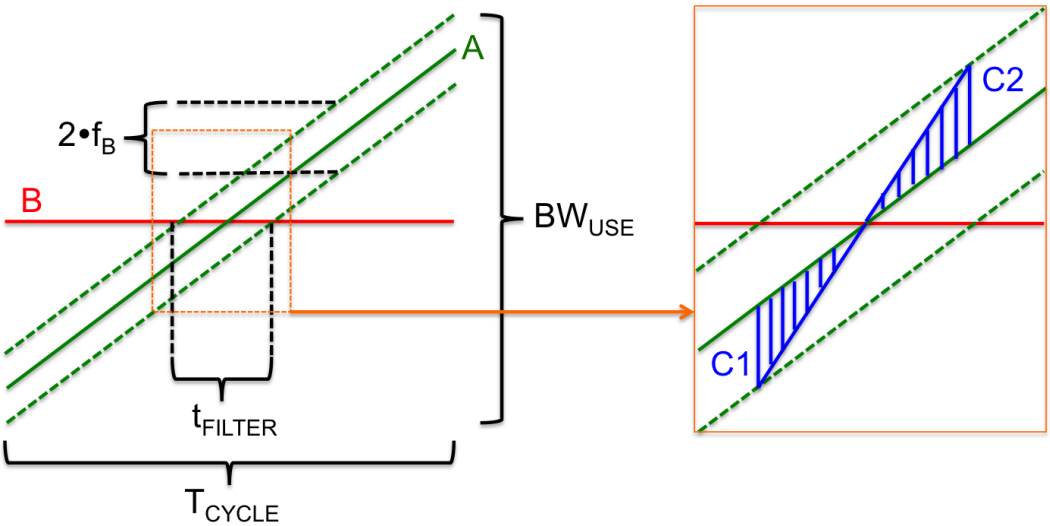

Fig. 3-1: LEFT: visualization of the limited time of interference (t_{FILTER})
RIGHT: Decorrelation by the mixing procedure (limited also in frequency)

The total estimated mitigation gain in the signal-to-interference ratio from antenna port up to the digitized data for an ideal mixer including a DFT with NFFT points [OprRoh] is

$$MG_{S/I} = \frac{BW_{USE}}{2 \times f_B} \times NFFT = \frac{BW_{USE}}{2 \times f_B} \times \frac{T_{CYCLE}}{t_s} \tag{3-1}$$

If the sampling time t_S is chosen to $\frac{1}{2 \times f_B}$, the sampling theory is satisfied and this results in

$$MG_{S/I} = \frac{BW_{USE}}{2 \times f_B} \frac{T_{CYCLE}}{\frac{1}{2 \times f_B}} = BW_{USE} \times T_{CYCLE} \tag{3-2}$$

In the case of a FMCW interfering signal and not just a CW signal, the total dwell time in the victim receiver filter t_{FILTER} (and by this the time per frequency bin in the FFT) can be further increased or decreased [Gop]. This effect can be taken into account by introducing the following scaling factor for $MG_{S/I}$

$$SF = \frac{\left| \frac{BW_{USE}}{T_{CYCLE}} \right|}{\left| \frac{BW_{USE}}{T_{CYCLE}} - \frac{BW_{INT}}{T_{INT}} \right|} \tag{3-3}$$

Where $MG_{S/I}$ is increased if both victim and interfering ramps have different slope signs (i.e time per frequency bin is further decreasing, resulting in less disturbed sampling points). On the other hand, SF is decreasing when both victim and interfering ramps have the same slope sign (i.e. time per frequency bin is increasing, with the effect to get more disturbed sampling points).

The key to this high gain of signal-to-interference ratio is

- The interference is limited to fewer sampling points.
- The sampled /relevant interference contribution to the overall signal is furthermore uncorrelated to the use-signal

Because the interfering signal is highly auto-correlated with itself, and if no I/Q-demodulator is used, the calculated gain versus interference is reduced further by up to 6dB (in voltage dimension the factor 2, i.e. $20\log_{10}(2)$ in dB). This effect is visualized in Fig.3-2.

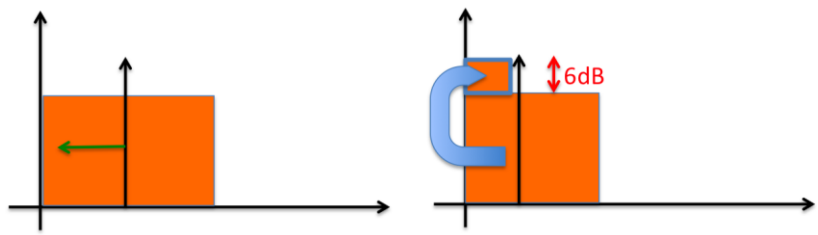

Fig. 3-2: Loose of 6dB in gain versus interference due to non-use of I/Q mixer in frequency domain

To demonstrate the equations (3-2) and (3-3), measurements have been performed for the single interferer case. Therefore an FMCW signal with 4 MHz BW and a cycle time of 0.1 ms is created and mixed with it's delayed version, sampled and Fourier transformed. This results in a target visible in the first row of the graphs in Fig. 3-3.

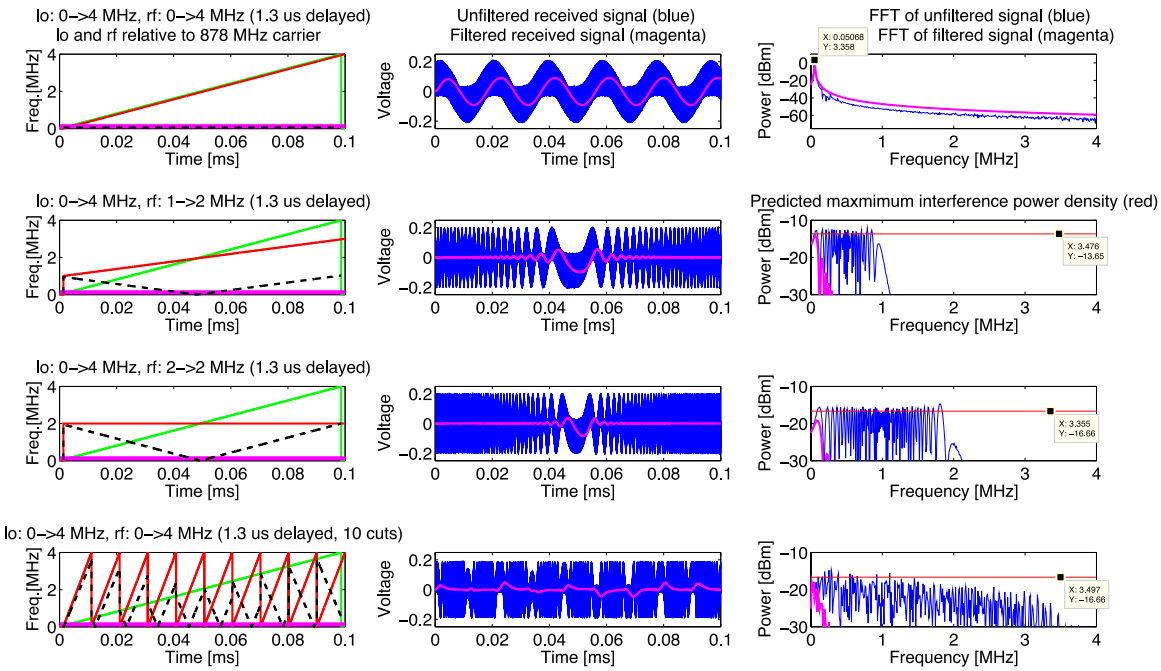

Fig. 3-3: Verification of the estimated interference floor in frequency domain. No I/Q data was used.
Left Column: Green=LO-signal, Red= RF-signal, Black-dotted=resulting mixer output frequencies, magenta=3dB-filter bandwidth (magenta also marks filtered signals in time and frequency domain)
Note: As anti-aliasing filter a Bessel 2nd order low-pass with 120 kHz cutoff is used

In the left column in Fig.3-3, the generated mixer output frequencies are plotted. Every time the black-dotted line (mixer output frequencies) comes close or below the magenta line (filter 3dB cut-off frequency), a peak in time domain becomes visible (middle column). These time domain signals can be transformed into frequency domain, where an interference floor is created which can reduce the dynamic range in a radar. The red line in the right column indicates the predicted interference power level in frequency domain due to the changing frequency slopes of the delayed received signal. The observed interference power level in frequency domain for this target peak is lowered by $MG_{S/I}$ including the scaling factor SF from row to row, until a CW interference is present in the second last row in Fig. 3-3. The last row in Fig. 3-3 is showing 10 transitions through the victim's anti aliasing filter, resulting in the same interference power level as for the CW interference case. For the CW interfering case we observe 20 dB gain in S/I, which corresponds to 4 MHz* 0.1 ms = 400 -> 26 dB gain - 6 dB(no I/Q data) = 20 dB. More details about the methodology to describe multiple interference effects can be found in deliverable D2.6.

3.2. Detection range in the presence of interference

Complete link budget in free space from interferer to victim radar with radiation patterns included can be calculated as follows

$$P_{RI} = \frac{P_{TI} \cdot G_{TXI} \cdot \left|C_{TI}(\Omega_{TI})\right|^2 \cdot G_{RX} \cdot \left|C_{RX}(\Omega_{RXI})\right|^2 \cdot c_0^2}{(4\pi)^2 R_I^2 f^2} \tag{3-4}$$

The radar equation can be also rewritten with normalized radiation patterns included

$$P_{RX} = \frac{P_{TX} \cdot G_{TXU} \cdot \left|C_{TX}(\Omega_{TX})\right|^2 \cdot G_{RX} \cdot \left|C_{RX}(\Omega_{RX})\right|^2 \cdot \sigma \cdot c_0^2}{(4\pi)^3 R^4 \cdot f^2} \tag{3-5}$$

Assuming the change in modulation frequency is small in relation to the carrier frequency, the signal to interference ratio including the complete interference mitigation gain $MG_{S/I}$ from antenna port up to the digitized, Fourier-transformed data is given by

$$\frac{S}{I} = \frac{P_{RX}}{P_{RI}} = \frac{P_{TX}}{P_{TI}} \cdot \frac{G_{TXU}}{G_{TXI}} \cdot \frac{R_I^2}{4\pi R^4} \cdot \left| \frac{\left|C_{TX}(\Omega_{TX})\right| \cdot \left|C_{RX}(\Omega_{RX})\right|}{\left|C_{TI}(\Omega_{TI})\right| \cdot \left|C_{RX}(\Omega_{RXI})\right|} \right|^2 \cdot \sigma \cdot MG_{S/I} \tag{3-6}$$

Legend for all equations:

P_{RI}	:	received power from disturbing radar
P_{RX}	:	received power from target
P_{TX}	:	transmit power of victim radar
P_{TI}	:	transmit power of disturbing radar
G_{RX}	:	victim receive antenna gain
G_{TXI}	:	disturbing radar transmit antenna gain
G_{TXU}	:	victim radar transmit antenna gain
C_{TX}	:	normalized radiation pattern of victim radar
Ω_{TX}	:	angle of emission of the useful signal from victim radar antenna
C_{TI}	:	normalized radiation pattern of disturbing radar
Ω_{TI}	:	angle of emission of the signal from disturbing radar antenna
C_{RX}	:	normalized radiation pattern of victim radar
Ω_{RX}	:	angle of incidence of the useful signal at victim radar antenna
σ	:	radar cross section of the target
R	:	distance from target to victim radar
R_I	:	distance from interferer to victim radar
$MG_{S/I}$	:	interference mitigation gain from antenna port up to the digitized data in frequency domain
f	:	carrier frequency
c_0	:	speed of light ($3*10^8$ m/s)

Rearranging equation (3-6) for R_I the maximum distance can be calculated, for which a disturbing radar may still detect a targets under given boundary conditions and one single propagation path (line of sight).

$$R_I = \sqrt{\frac{S}{I} \cdot \frac{P_{TI}}{P_{TX}} \cdot \frac{G_{TXU}}{G_{TXI}} \cdot 4pR^4 \cdot \left| \frac{|C_{TI}(W_{TI})| \cdot |C_{RX}(W_{RXI})|}{|C_{TX}(W_{TX})| \cdot |C_{RX}(W_{RX})|} \right|^2 \cdot \frac{1}{s \cdot MG_{S/I}}} \tag{3-7}$$

For a target in 200m distance with an RCS of $10m^2$ a processing gain of 59.5dB (150MHz bandwidth, 6ms ramp duration), omni-directional antennas, a desired minimum signal-to-interference ratio of 12 dB and a transmit power of 20dBm EIRP pursuant to the respective ETSI standards for both victim and interference radar, the minimum distance an interferer has to approach the observing radar to suppress the detection of the 10 dBsm target is about 188 m for interference occurring within the main beam; the interferer is assumed to operate in CW mode. Fig.3-4 illustrates the borders for possible target detection for several targets with RCS from 0 to 30 dBsm ($MG_{S/I}$ is named G_P in this figure). The formula in 3-7 will be verified in near future by practical experiments conducted by the MOSARIM project partners. It maybe necessary to adapt R^4 to a lower value, because targets cannot be assumed to be ideally point targets but have finite apertures which may interact with the beamwidth of the radars (i.e. target size larger then the beamwidth in the near vicinity).

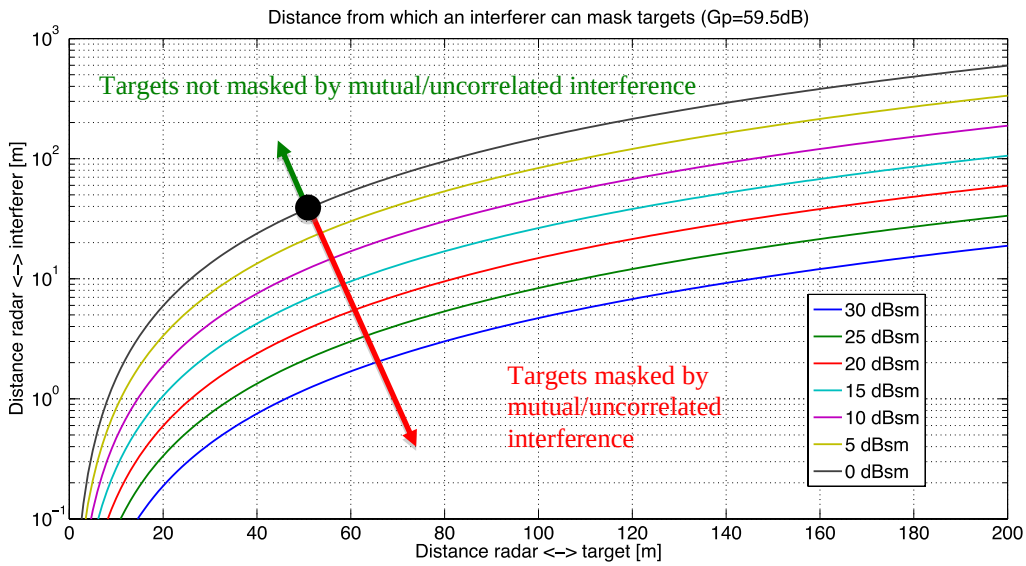

Fig. 3-4: Borders for target detection based on equation 2-11

3.3. Example of a worst case scenario

Equation (3-7) is especially useful to find and define relevant interfering scenarios. Fig. 3-5 is showing a possible worst case situation for the single interfering case.

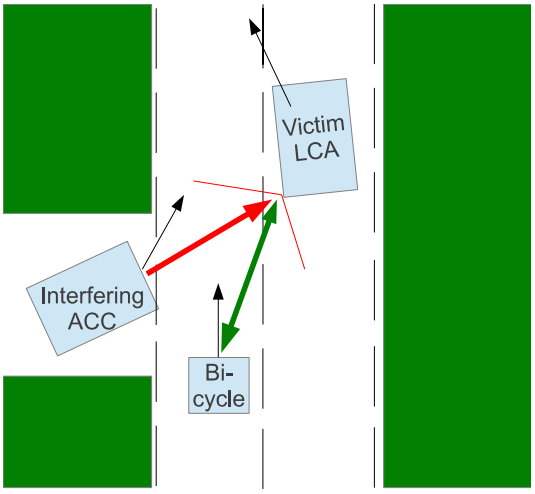

Fig. 3-5: A small target is approaching while an LCA / BSD is disturbed by an ACC

Assuming that the bicycle does not shield the ACC yet and both interfering car and bicycle have the same distance to the LCA (about 10 m). The LCA has the same parameters as described in section 3.2, both LCA and ACC have the same EIRP of 20 dBm. The scaling factor for the interference mitigation gain is assumed to be around 1. For these parameters, Fig.3-4 shows us that the bicycle is assumed to be 12 dB above the noise level (with IQ-receiver assumed). So it could be expected that the bicycle is around 6 dB above the noise level in worst-case.

4. Modeling of relevant propagation effects

4.1. Two-path propagation

In an environment with only a victim radar and an interference radar on a road surface a two-way propagation exists: one direct way (line-of-sight) and one indirect way with reflection via the road surface. Fig.4-1 shows the received power at the antenna port if a two-path propagation between two antennas with a height of 0.5 m above the ground is assumed. Fig.4-1 shows the received power at the antenna port if a two-path propagation between two antennas with a height of 0.5 m above the ground is assumed.

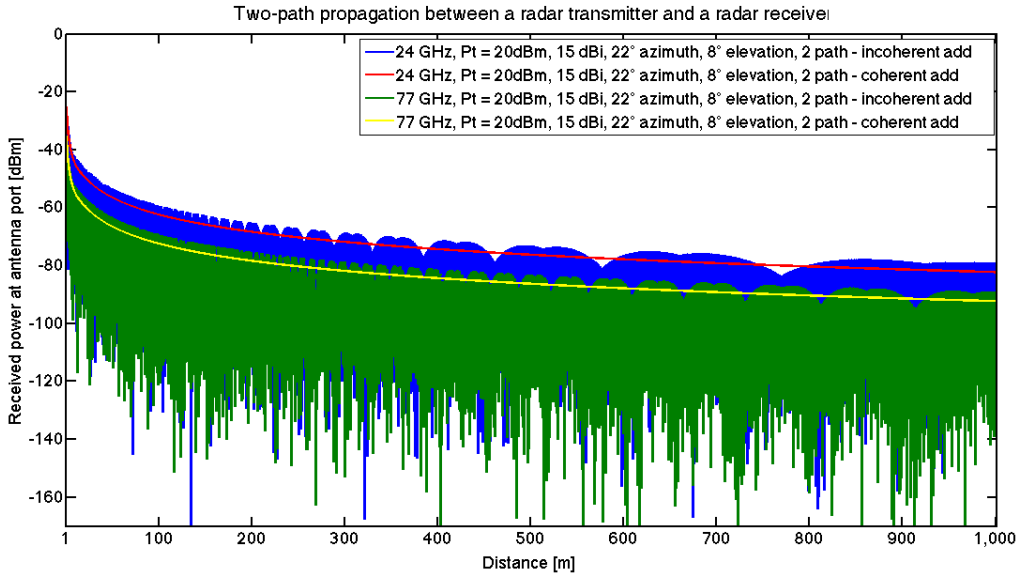

Fig. 4-1: Fading at receive antenna due to two-path propagation effect

4.2. Multipath propagation

During the test campaign in a tunnel in Utrecht, the Netherlands, on January 14th, 2012 measurements have been performed to check the capability of the used wave propagation simulation engine to reproduce the propagation of energy in an environment with a high amount of multipaths. These measurements in a tunnel were also of special interest for the project, because a significant lower path loss was expected in comparison to free-space propagation or e.g. the propagation above a PEC half-plane. This scenario is likely to be a worst case propagation scenario.

The measurements have been performed for a continuous wave (CW) frequency at 24.125 GHz and for all combinations of linear polarization(HH, HV, VH, VV). A vehicle's trunk was equipped with a signal generator and a fixed antenna (Fig.4-2b). On receive side, a tripod device was equipped with a receiving antenna, followed by a low noise amplifier and a spectrum analyzer to measure the received power (Fig.4-2a).
The street was sampled in steps of 100m each. The spectrum analyzer was first reset and then set to max-hold 10m before up to 10m behind each sampling point.

Fig. 4-2a: non-coherent receiver, max-hold

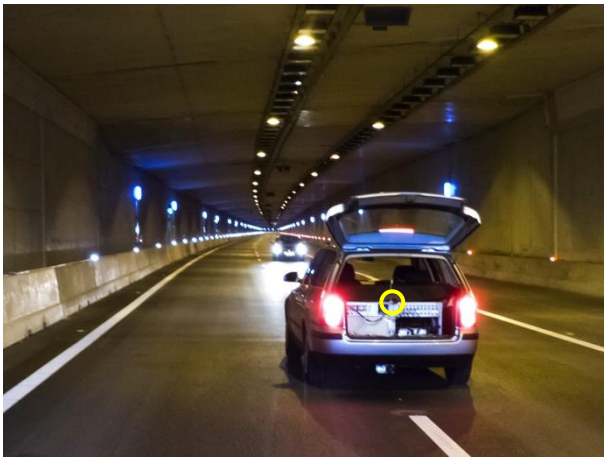

Fig. 4-2b: CW transmitter (24.125 GHz)

Fig.4-3 shows the technical drawing of the tunnel in profile cut.

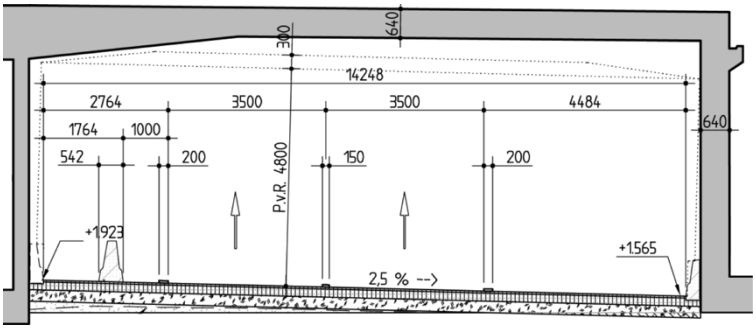

Fig. 4-3: Profile of the tunnel

The measurement results are visualized in Fig.4-4 and show a decoupling for cross-polarization of about 20dB.

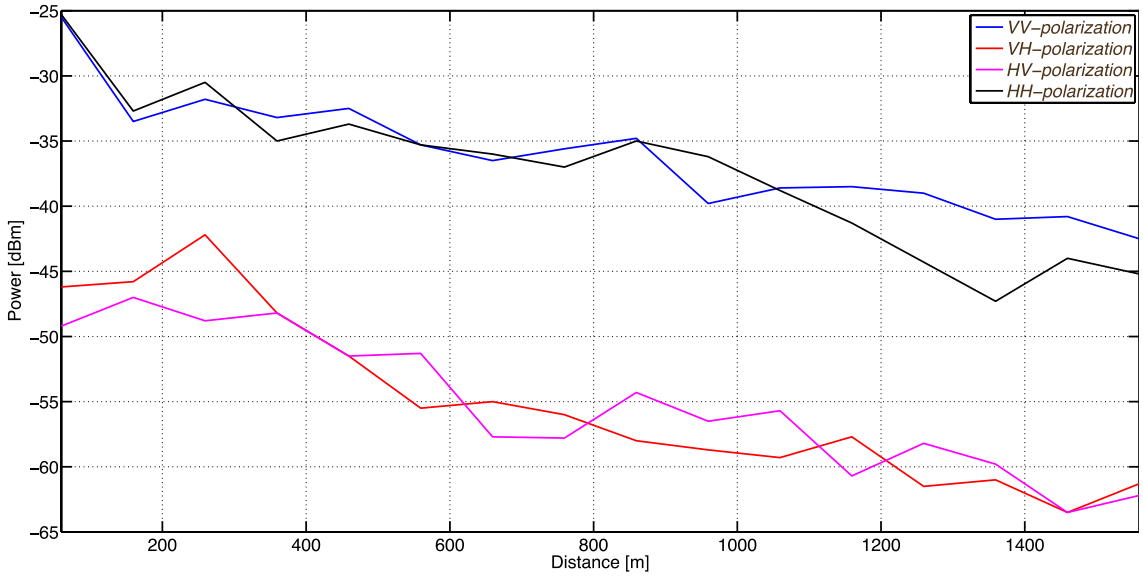

Fig. 4-4: Recorded (incoherent) receive power, max hold used within +/- 10 m at each 100m mark of the tunnel

The tunnel is slightly bended towards the south end. Above 200m, the energy is already almost equal distributed, so the bending effect is assumed to be negligible and is not considered while modeling the tunnel. (In deliverable D1.7 [D17] this behavior is illustrated

while investigating the interference potential of fixed radar device in a tunnel by simulation). Fig. 4-5 shows the polygon-based model of the tunnel, the walls, barrier and ceiling are modeled as concrete. Table 4-1 shows the used material parameters for simulation.

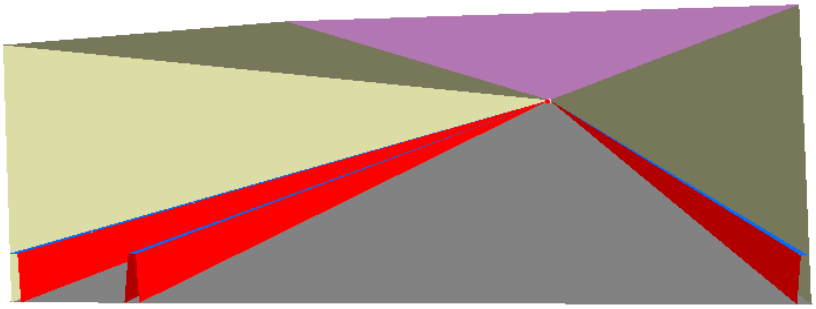

Fig. 4-5: Polygon based model of the tunnel in Utrecht

Asphalt/Concrete	ε'=2.52 ε''=0.6, σ=0.5 mm (standard deviation of surface height), $\sigma < \lambda_0/(32 \cos(\theta_i))$? if yes => flat surface for all angles of incidence > ~40° based on Fraunhofer criterion. All other propagation paths have additional losses due to surface roughness and are considered by modified Fresnel reflection factors [Geng1]. (0° is perpendicular illumination of the street)
Concrete	ε'= 2.52, ε''= 0,431 σ << 0.5 mm -> negligible based on Fraunhofer criterion

Tab. 4-1: Material parameters used for ray-tracing simulation

Fig.4-6 shows the comparison of the incoherent measurements using max hold and a simulation with incoherent summation of paths for VV polarization. In addition, free-space propagation and the two-path model are plotted for comparison. The simulation results have been normalized to the first measurement point for better comparison..

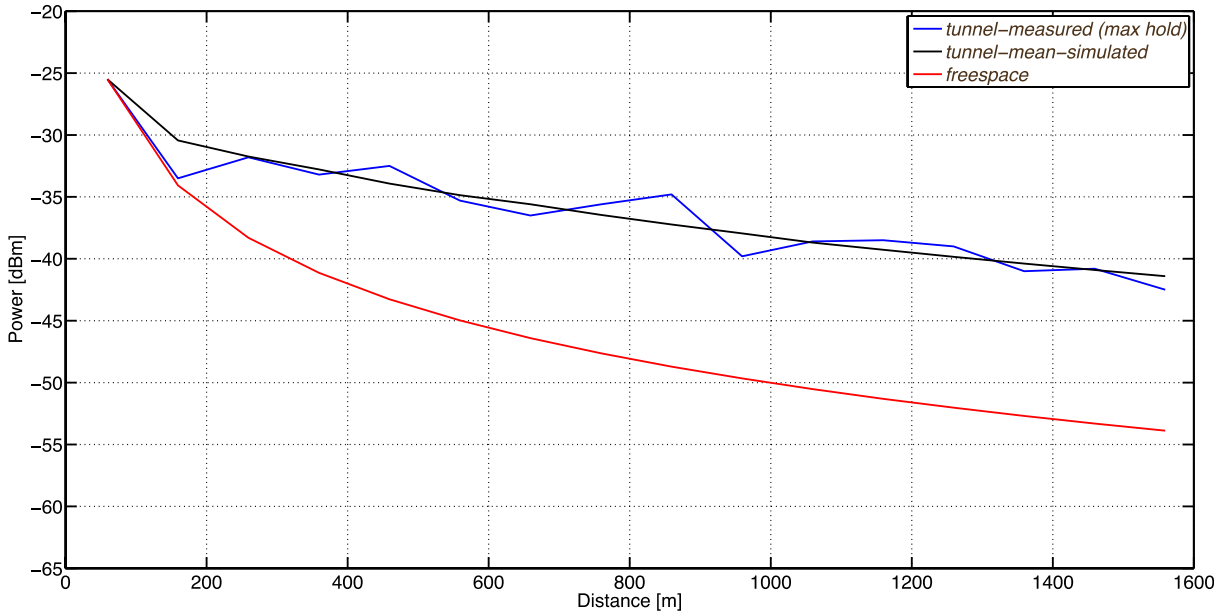

Fig. 4-6: Measurement compared to simulations (VV-polarization)

Important results of these measurements:
The roll off in this tunnel can be described quiet well by **10~12dB/decade in distance** were normal free-space path loss has 20dB/decade in distance of signal attenuation. Also the used simulation tool seems to be adequate enough to reproduce real world measurements for co-polarization. The simulation of cross polarization (i.e. VH or HV) did not lead to a significant correlation with measurements, because polarization changes in the simulator are always connected to dihedral-like structures (if a polygon is defined as a reflector). Nevertheless scatterers or scattering centers have the ability to change the polarization in a random or deterministic way, but were not used for modelling due to the fact that the path loss behaviour in principle is already investigated for co-polarization and can be used for worst-case interference estimations.

4.3. Shielding

The shielding by road participants is also a key aspect, which has to be considered, and a more sophisticated simulation model is able to reproduce such effects.
Because the ray-tracing tool used in the simulation tool chain supports multiple reflections, edge-diffractions based on the uniform theory of diffraction and mixtures of both, the basic shielding functionality is already built in and thus automatically taken into account. Fig.4-7 to Fig.4-10 show exemplary simulations of an easy shielding scenario for 24.125 and 76.5 GHz (polarizations: tt=vv; hh=pp). A car is moved from the transmitter to the receiver and in such a way that line of sight is always blocked by the car. The value of shielding was calculated by creating the relation between the undisturbed propagation (free-space, no two-path assumed here) and the propagation with the shielding car in between, assuming an empty street and omni-directional antennas.

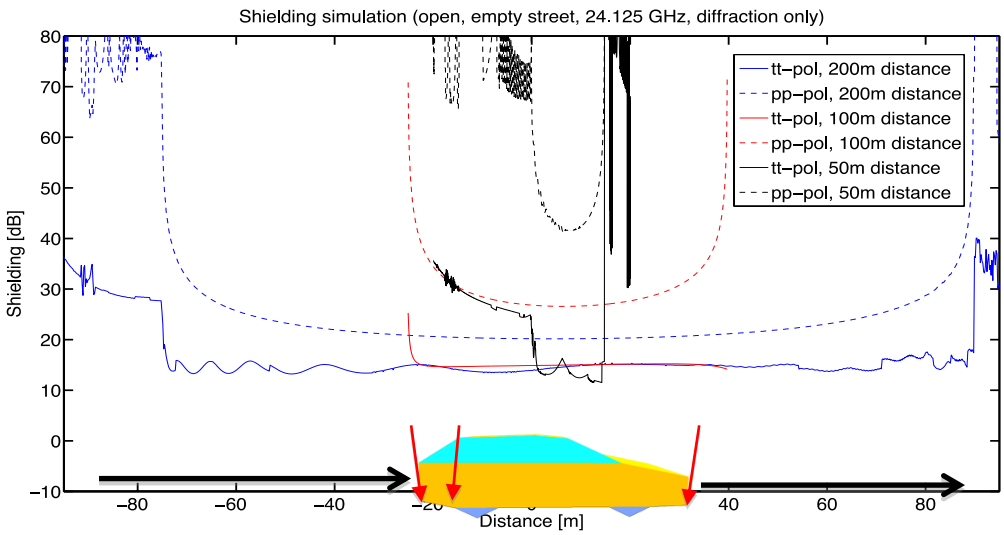

Fig. 4-7: Shielding behavior, no reflections from the street are allowed (diffraction of car only)

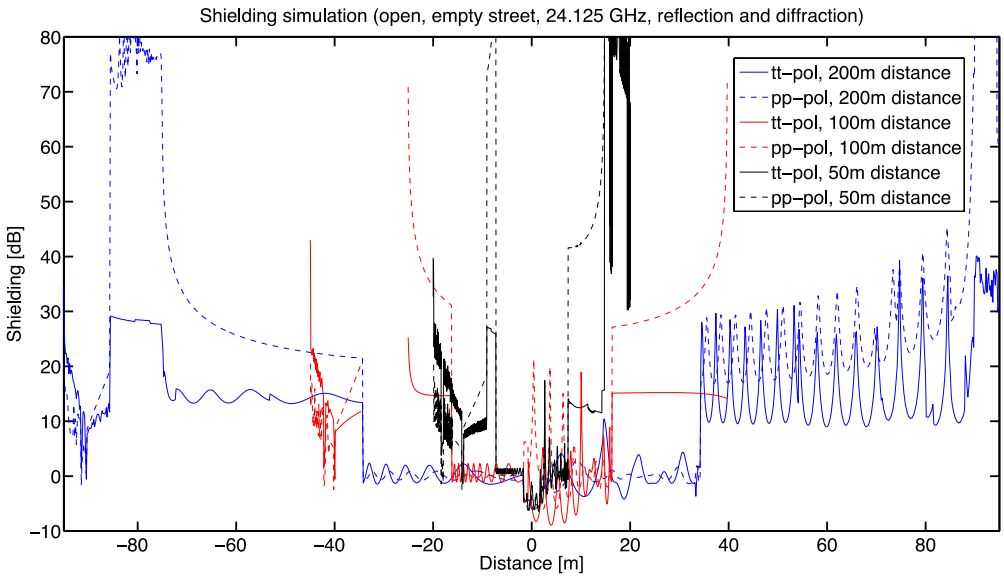

Fig. 4-8: Shielding behavior, reflection, diffraction and combinations of both are allowed.

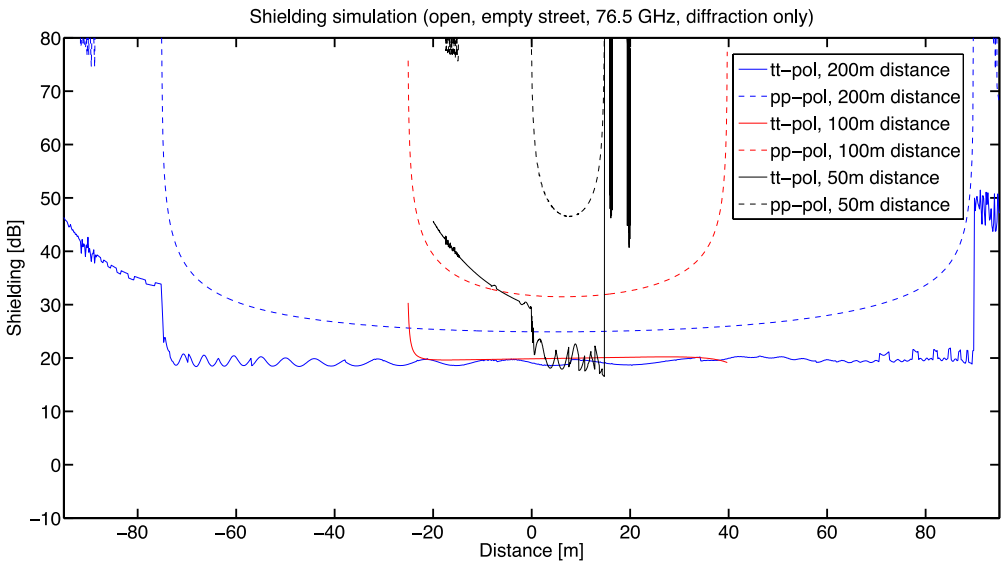

Fig. 4-9: Shielding behavior, no reflections from the street are allowed (diffraction of car only)

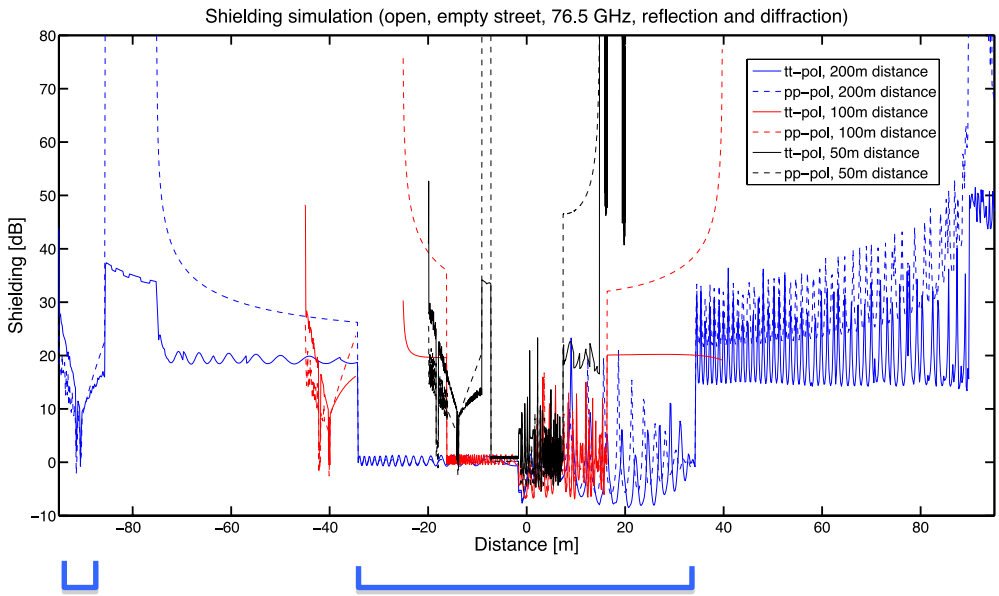

Areas, which are dominated by reflections or combinations of reflections and diffractions (mixed paths)

Fig. 4-10: Shielding behavior, reflection, diffraction and combinations of both are allowed.

The materials used for these simulations were metal for the car outline, glass for the car window (60 GHz, e' =5.29, tan δ = 0.048; 5 GHz, e' = 6, tan δ = 0.01) and asphalt/concrete as it is described in section 4.2 for the modeling of the tunnel.

If only reflections were allowed, the areas marked below Fig. 4-10 will still be present, but without fading effects (only one path is found, or two symmetric paths e.g.). Mixed paths (reflections in combination with diffractions) lead to more propagation paths and cause the fading in the marked areas. The same effect can be recognized for 24 and 77GHz. In relation to frees-pace propagation, or even in relation to the two-path model (maximum of +6dB in relation to free-space), the car within the simulation can have a negative shielding for some positions. The reason for that is, that the car focuses energy in the direction of the receiving

antenna. If this effect found in the simulations can be confirmed in practice is still to be determined.
In the areas where diffraction is dominant, fading also occurs. When comparing Fig. 4-8 and Fig.4-10 it can be seen that fading effects result from mixed paths (blue curve, right side), but can also be a result of diffracted paths (blue curve, left side).
A very smooth line (negligible fading, especially for the horizontal polarization) is an indicator for a single, but dominant propagation path.

When comparing the overall shielding behavior for 24/77 GHz, the main differences are a faster fading behavior for 77 GHz and a higher shielding (~ +5dB) for 77 GHz in areas, where diffraction is dominant.

5. Road scenarios considered in this deliverable

In chapter 4 it was demonstrated, that the general ability to consider multi path effects as well as shielding effects is given by the present simulation tool. In chapter 5 common road scenarios are investigated on their ability to preserve energy (tunnel scenario) and also complete scenarios including environment and road participants (cars) are considered.

In this chapter the received interference power at the antenna port is calculated for a simple test setup. The complexity of this test scenario is continuously increased and the results are displayed for the different frequency ranges and exemplary antennas. All scenarios contain only one victim car and one interfering car, both equipped with 3 radars (24 GHz, 1 ACC, 2 LCA) or 1 radar (77 GHz, ACC). Fig. 5-0a shows the used antennas together with a car model in a top view. Fig. 5-0b shows the test setup that is the basis for scenario A to F, and Fig. 5-0c shows the test setup that is the basis for scenario G-H.

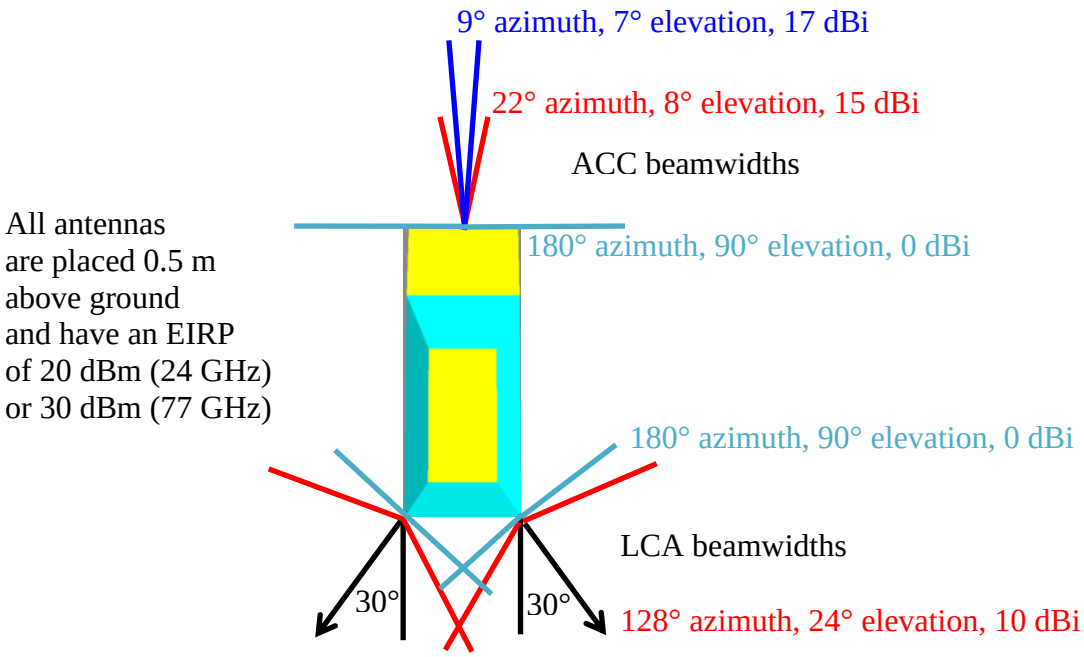

Fig. 5-0a: Overview of the used antennas and their placement

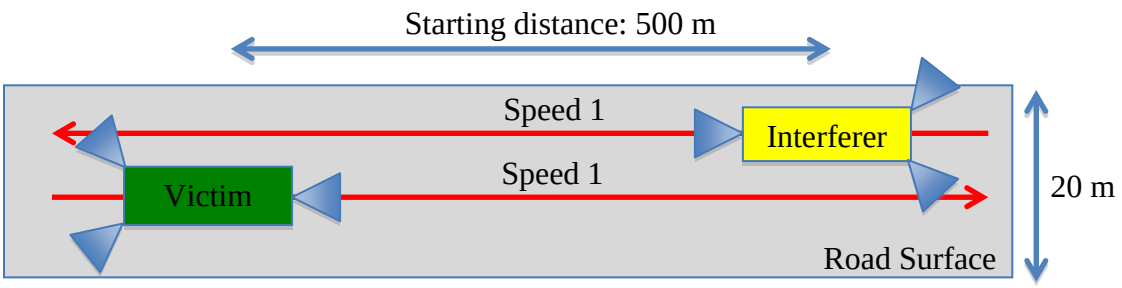

Fig. 5-0b: Basic setup for scenarios A-F

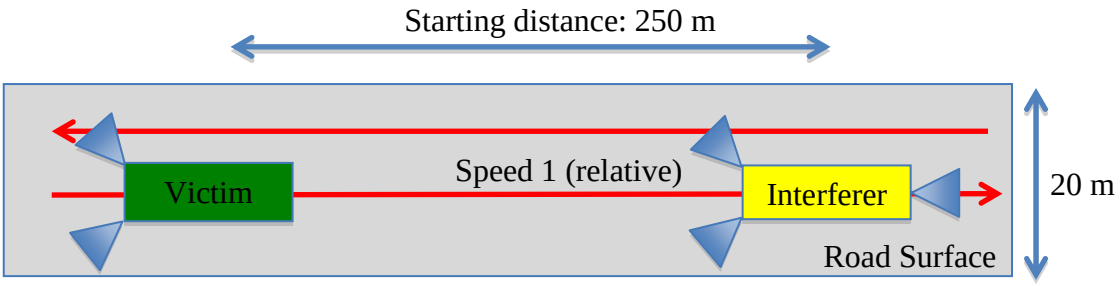

Fig. 5-0c: Basic setup for scenario G-H

In the following five different scenarios are briefly presented. They are used to check if the gathered scenarios out of deliverable D2.2 [D12] can be seen as worst-case scenarios for the single interference case. If this is true, equation (3-7) can be used to estimate the distance an interferer has to approach a victim radar to become relevant.

5.1.A: Close passing

Two cars are passing each other in a near distance of 1 m. The scenario is shown in Fig. 5-1. The starting distance is 500 m. The cars have the same speed and meet at 250 m distance.

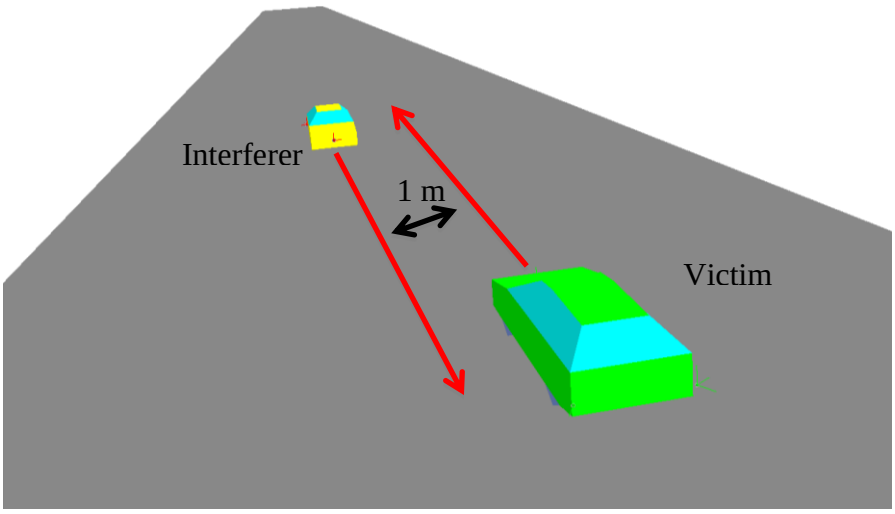

Fig. 5-1: Scenario A, a basic scenario. No shielding, two-path only

5.2.B: Close passing – additional shielding / reflection by cars

Scenario A is modified by placing cars in 50 m steps in front and after the victim / interferer.

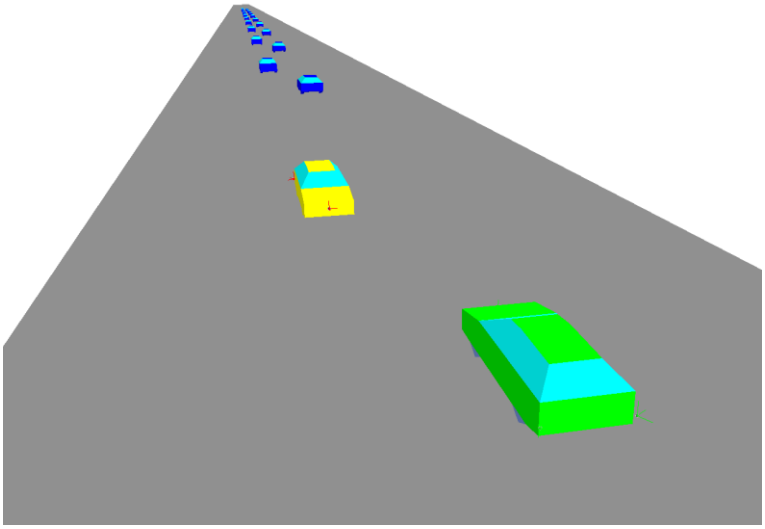

Fig. 5-2: Scenario B, influence of road participants in rural environment (a few multipaths occur)

5.3.C: Close passing – canyon

Scenario B is changed by adding concrete walls on both sides of the street to increase the number of multipaths. The walls are covering 500 m of the street.

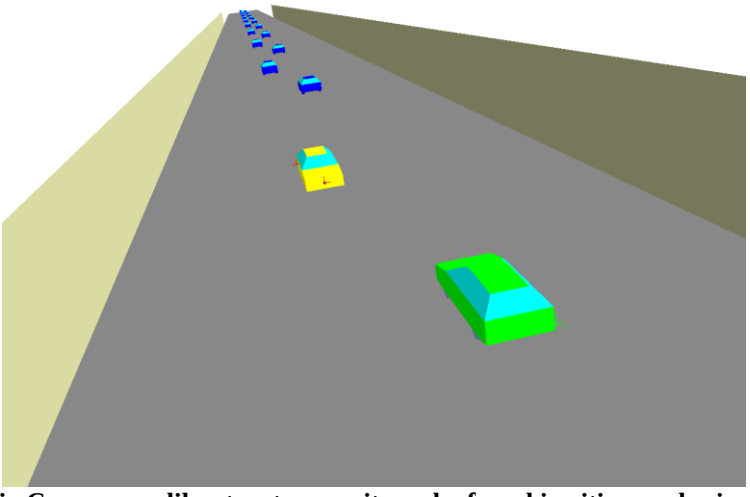

Fig. 5-3: Scenario C, a canyon like structure, as it can be found in cities or also in nature

5.4.D: Close passing – tunnel

The canyon from scenario C is now changed into a tunnel to further increase the amount of multi-paths.

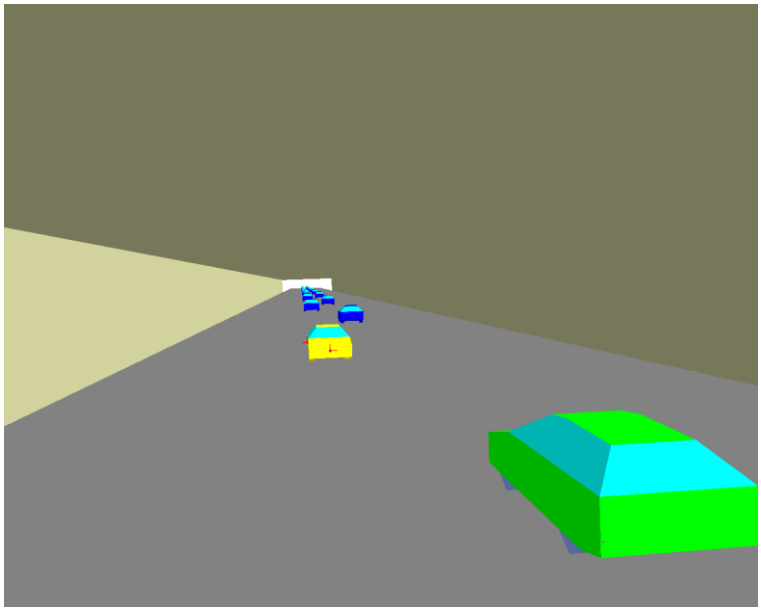

Fig. 5-4: Scenario D, a tunnel with centered driving lanes

5.5.E: Enlarged passing distance

Scenario D is changed by enlarging the lateral distance between the victim car and the interferer car from 1 m to 3.5 m.

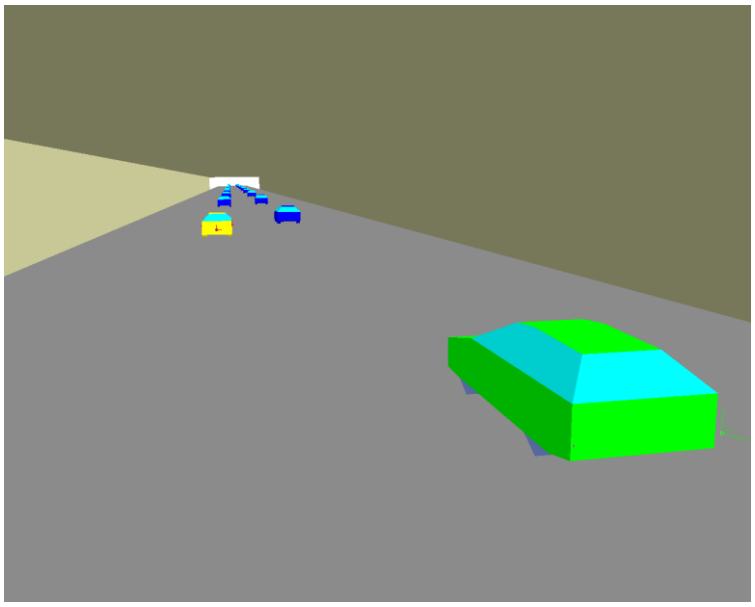

Fig. 5-5: Scenario E, more space between driving lanes in the tunnel

5.6.F: Close passing with guardrail

A guardrail is inserted in addition to scenario-setup D.

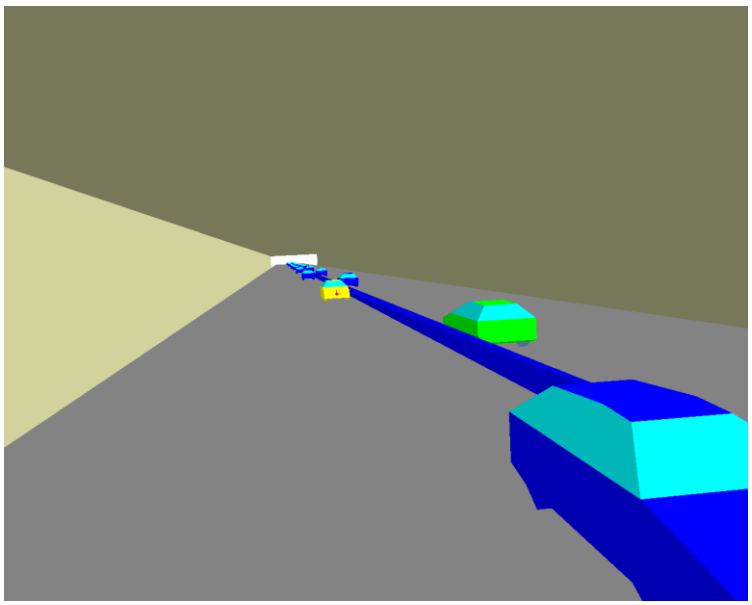

Fig. 5-6: The guardrail in a tunnel effectively shields interference from oncoming vehicles.

5.7.G: Tailgating a car in front

Victim and interferer car are now placed on the same lane. One of both is fixed in position, and the other is approaching from 250 m distance.

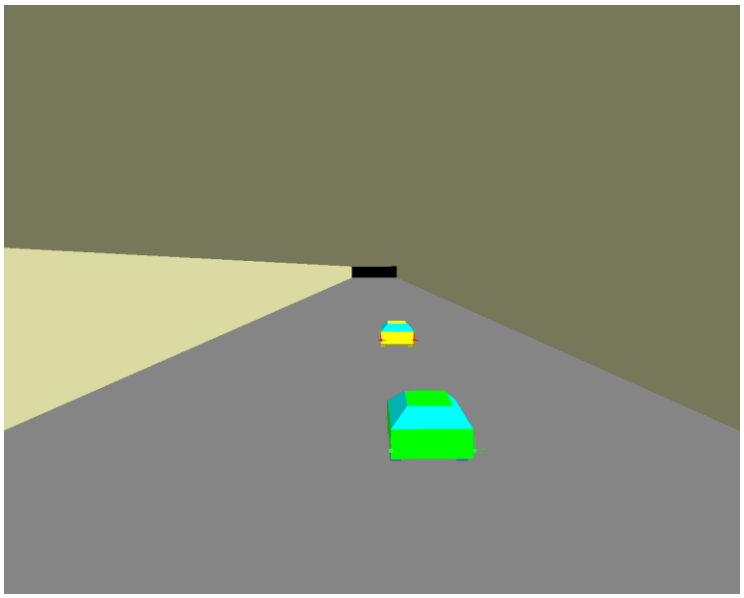

Fig. 5-7: Approaching a car on same lane

5.8.H: Tailgating a car in front with guardrail

The same as described in scenario G, just a guardrail is added.

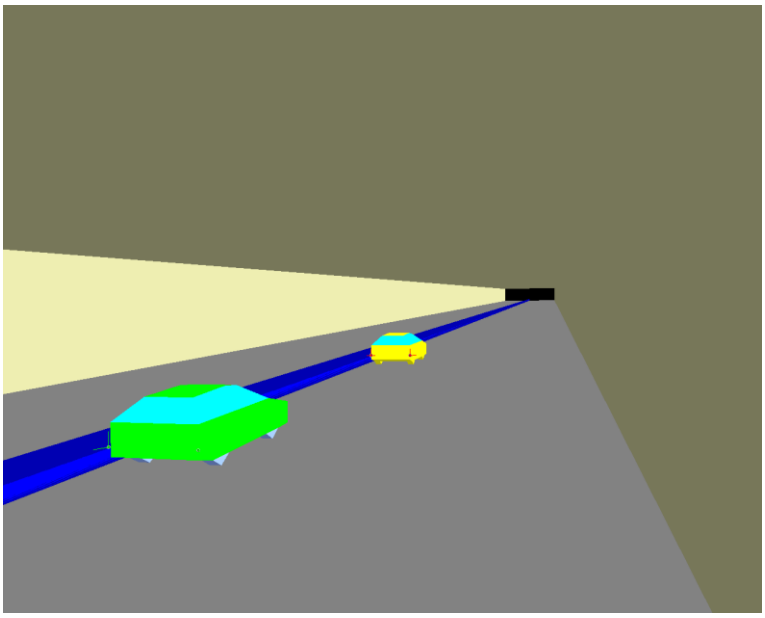

Fig. 5-8: An additional guard rail is inserted in relation to Fig. 5-7

6. Simulation results

The results are coded in the following way:

Scenario ID: victim radar <-> interfering radar , additional information.

E.g. A: ACC <-> LCA-BR/BL would mean it displays the incoherent addition of interference powers from two LCA radars (BR= back right mounted, BL= back left mounted). The environment used is scenario A.

If no extra information about polarization for receive or transmit antennas is mentioned within graphics, always horizontal polarization (hh-pol. or also called pp-pol.) is plotted.

6.1. Results for 24 GHz ACC operation

Fig. 6-1a shows the incoherent received interference power at the victim receiver's antenna port. For this simulation run only the ACC radars are active.

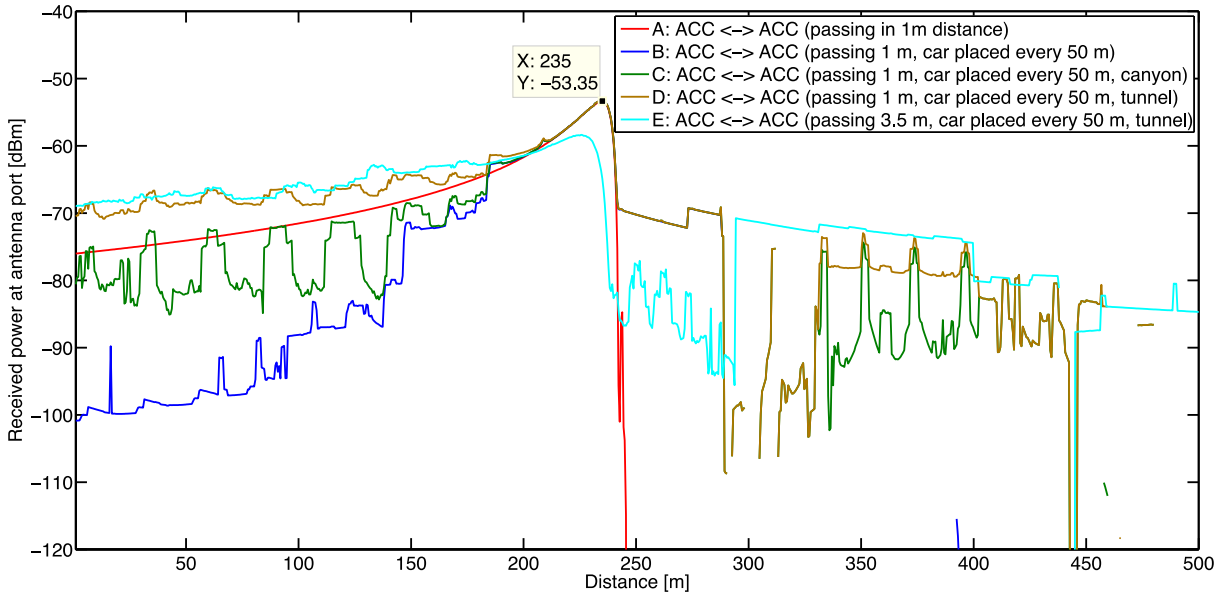

Fig. 6-1a: The received interference power at the victim antenna port as a function of a driven distance. Both cars are passing each other at 250 m.

When observing Fig. 6-1 it can be clearly seen that there is no difference between the five scenario setups A-E in terms of maximum incoherent received interference power. Additional cars on the street without walls or ceilings lead to a great shielding effect for larger distances (blue curve, rural). Remarkable is, that the canyon (green) only brings the power levels back from the rural scenario (blue) to the two-path propagation case (red), although we used optimal polarization for the propagation in H-plane (hard polarization for outer car edges). The increase of the distance between the driving lane leads to a significant reduction of the maximum received interference power due to the smaller overlapping of the two radar main beam lobes. On the other hand, the received interference power in greater distances is increased, because the number of possible propagation paths between the cars is also increased.

Fig. 6-1b shows the aggregated incoherent received interference power at the 24 GHz victim ACC radar which is caused by the both LCA sensors of the interfering car in front of the victim car. Basis for the simulations are scenarios G and H. In near vicinity the antenna beam width helps to mitigate interference power in relation to a fictive omni-directional antenna with still the same antenna gain. The guardrail increased the received interference power for large and medium distances.

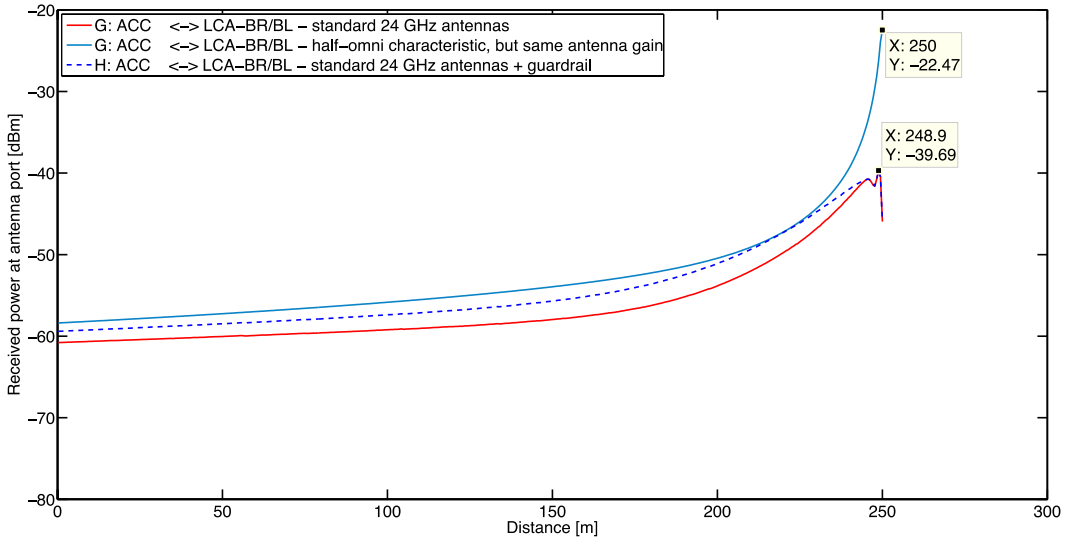

Fig. 6-1b: The Antenna beamwidths effectively reduce the received power in near vicinity. All radars are operating at 24.125 GHz

6.2. Results for 24 GHz LCA operation

Fig. 6-2a shows the incoherent received interference power at the victim receiver's antenna port for horizontal polarization on transmit and receive. For this simulation run it is assumed that only LCA radars are active. Both victim LCA radars receive the incoherent sum of both interfering LCA radars.

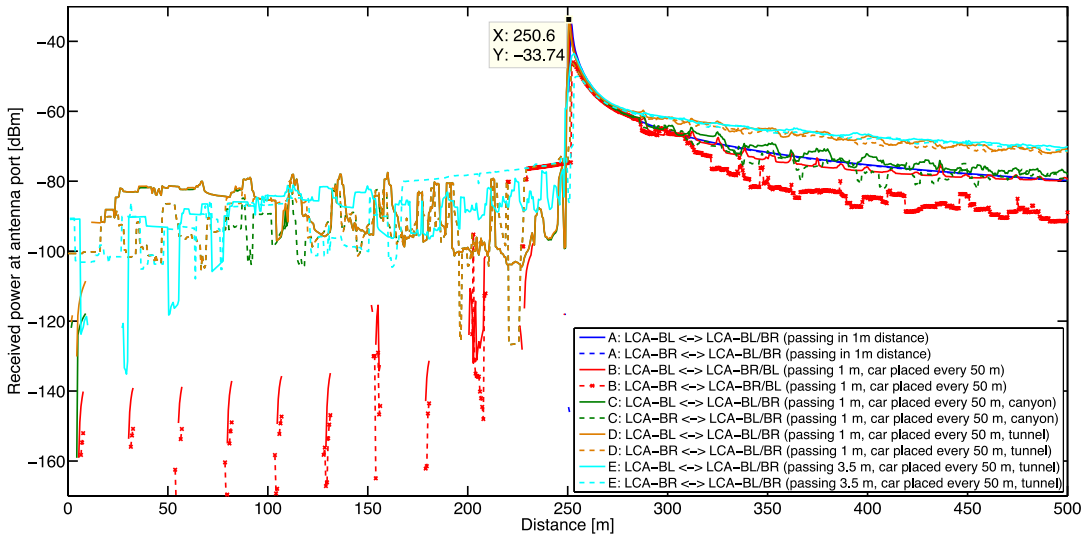

Fig. 6-2a: The maximum received interference power is clearly be dominated by the line of sight / two-path propagation in near vicinity. All radars are operating at 24.125 GHz

We see almost the same behavior as in section 6.1, but the maximum power levels are slightly higher (-33.74 dBm at the antenna port of an LCA in Fig. 6-2a, -39.69 dBm at the antenna port of the ACC in Fig. 6-1b). For the ACC versus ACC case we get about 20 dB less received interference power in relation to the simulations where LCA/BSD is included. The reason for this is, that –practically speaking- the ACC radars can never come close to each other AND disturb each other, while their main beams are overlapping or crossing. LCA radars come close to each other quite often, as well as they disturb each other mainly in their main beams (e.g. if vehicles are passing each other as given in the example scenarios within this document).

Additionally, the shielding potential of cars will be reduced if the antenna beam width increases.

The basis for these results in Fig. 6-2b is scenario G, where victim and interfering cars have swapped their positions. The graphic shows the received incoherent interference power caused from the ACC at the both LCAs, when increasing the distance between the both vehicles. Because the antenna setup is symmetrical, both received interference powers must have the same level. The received interference power drops about 20 dB for a 250 m drive in the tunnel.

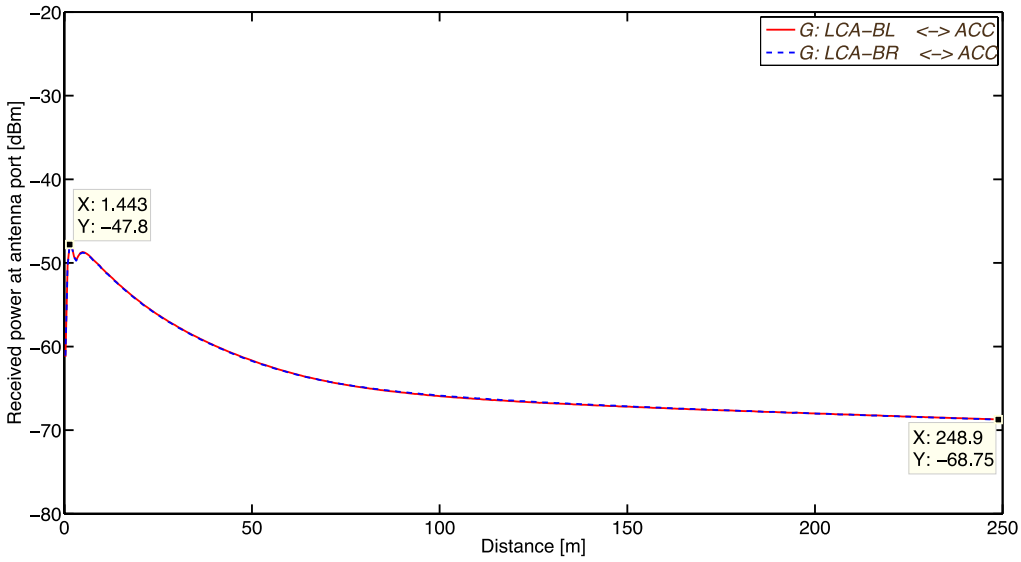

Fig. 6-2b: Received interference power at both LCAs, all radars are operating at 24.125 GHz

6.3. Results for 77 GHz ACC operation

For the 77 GHz region, we focus on scenario D and F, with and without a guardrail between the two driving lanes (as shown in Fig. 5-6). The guardrail starts from the ground and ends 20 cm above the involved antennas. Both variants are simulated for all co-polarizations and the result is shown in Fig. 6-3.

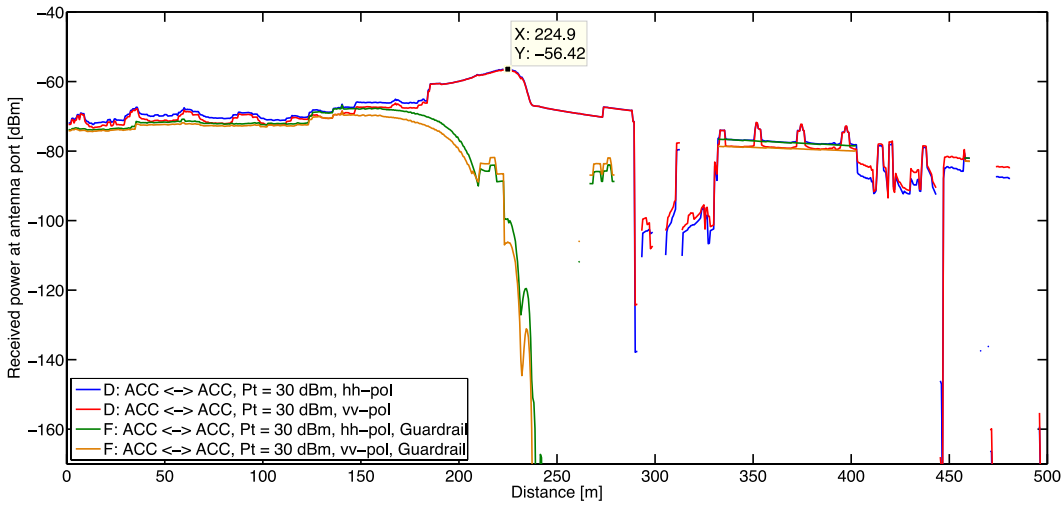

Fig. 6-3: The incoherent received interference power from one single ACC radar for co-polarizations

Due to the narrow main beam of ACC radars, strong interference levels on straight streets are rather unlikely. A guardrail or concrete wall starting from the ground can effectively shield interference caused by oncoming traffic. Guardrails starting with some space above ground still allow strong propagation paths and give about 3 dB less interference power compared to scenario A conditions.

6.4. Incoherent versus coherent received interference power

Fig. 6-4a and Fig. 6-4b show the incoherent and coherent received interference powers for scenario D, where all six 24 GHz radars are considered. The coherent summation of paths does not change the practical worst-case interference power levels significantly in this example. The change in displayed power levels due to coherent received signals/interference is dominated by a few, but strongest path-contributions, if they exist.

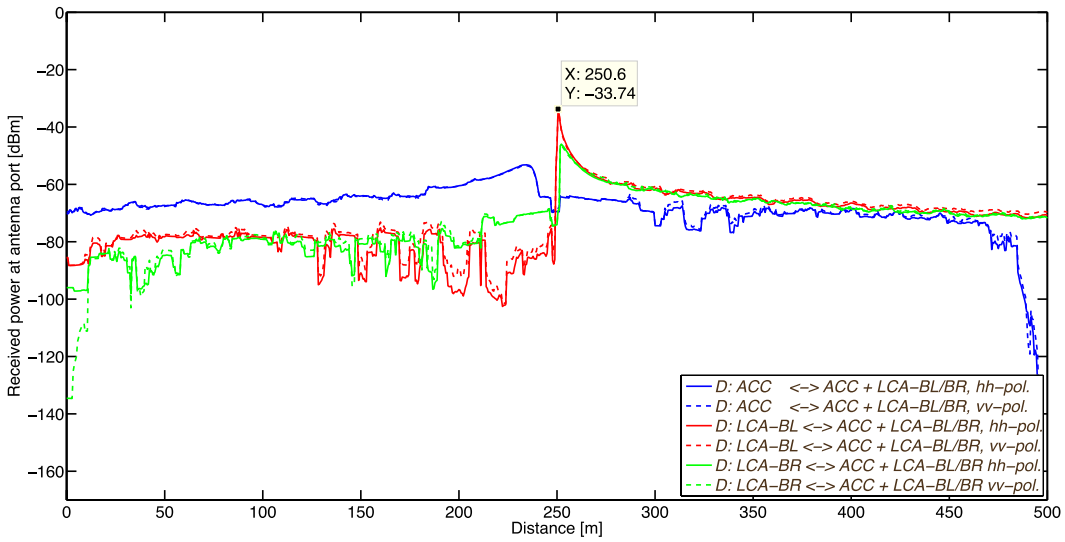

Fig. 6-4a: Maximum received interference power in a tunnel scenario due to three disturbing 24 GHz radars

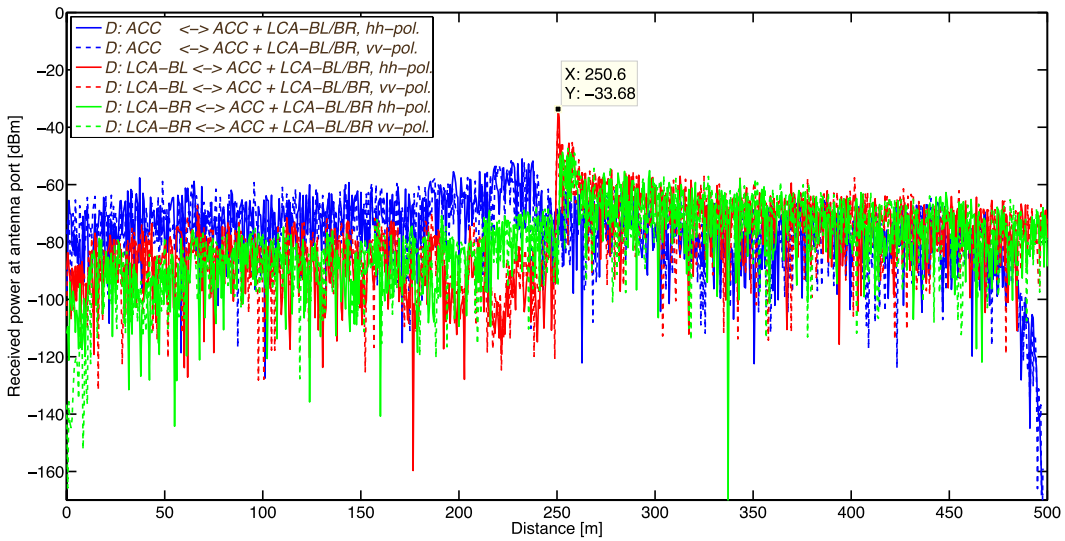

Fig. 6-4b: Increased maximum interference power level by coherent adding up of the 24 GHz radars.

7. Conclusions

Changes in the simulation tool-chain are depicted in chapter 2, followed by a demonstration of wave-propagation effects within the simulator in chapter 4. The capability to consider these propagation effects makes it possible to use this simulator for the investigations defined in this deliverable.

Due to the high amount of different radar systems it was necessary to derive simple equations to estimate the interference floor in the frequency domain after the FFT. In chapter 3 some equations were given which can be used to estimate the interference floor (eq. (3-2)(3-3)) as well as to estimate problematic constellations of radar, target and interferer with respect to the most important parameters (eq.(3-7)).

From all simulation-exercises running with single interference cases performed in this deliverable, it can be concluded that the line-of-sight is dominating if present.
Only for energy-focusing environments like tunnels, street- or natural canyons we observe a higher received interference power in comparison to the free-space/ two-path model due to these focusing or canalization effects. However, the absolute maximum received interference power occurs in a near distance, whereby the two-path propagation model and antenna patterns are sufficient to describe the wave propagation.

Based on these results, the scenarios from deliverable D1.2 can be assumed to be worst-case for the single interferer scenarios. The received mutual interference power levels are also not high enough to drive the high frequency circuits of the FM receivers into compression or saturation.
It turns out that sensors with wider antenna beam width (e.g. LCA, BSD, but also similar front mounted radars) are more susceptible to interference than radars with a narrow beam width (e.g. ACC). Radars with a narrow beam width have the advantage to get only interfered by the few targets, equipped with radars, they are actually observing, what provides higher signal-to-interference ratios by reducing the aggregated received interference power as well as the chance to be exposed to interference.

If the maximum possible interference levels for the *single entry* case are to be estimated, there is no need for complex wave propagation simulations. It is sufficient to apply a two-path model and the nearest line-of-sight connection between victim radar and interfering radar.
The capability to simulate interference effects in time domain is given and demonstrated within deliverable D3.6, whereby interference mitigation methods are applied to detect, avoid or eliminate interference effects.

An important step towards a better understanding what really happens if all cars on the road are equipped with radars, is included within deliverable D2.6. Here independent and realistic street scenarios are applied and their corresponding frequency distributions will be derived, allowing to estimate mean and worst-case interference power levels.

8. References

[D22] The MOSARIM Consortium, ”Generation of an interference susceptibility model for the different radar principles,” Workpackage: Simulation of Radar Interference Mechanisms, www.mosarim.eu, June 2010

[D24] The MOSARIM Consortium, ”Simulation setup assessment: interferer – free space propagation – victim radar,” Workpackage: Simulation of Radar Interference Mechanisms, www.mosarim.eu, June 2010

[D12] The MOSARIM Consortium, ”Specification of relevant scenarios, applications and traffic conditions,” Workpackage: General Interference Risk Assessment, www.mosarim.eu, June 2010

[OprRoh] D. Oprisan, H. Rohling, ”Analysis of Mutual Interference between Automotive Radar Systems,” International Radar Symposium (IRS), 2005, Berlin, Germany, Sep. 2005

[Gop] M. Goppelt, H.-L. Bleocher, W. Menzel, ”Analytical investigation of mutual interference between automotive FMCW radar sensors,” Microwave Conference (GeMIC), 2011 Germany, Mar. 2011

[Geng1] Geng, N., Wiesbeck, W., “Planungsmethoden für die Mobilkommunikation: Funknetzplanung unter realen physikalischen Ausbreitungsbedingungen“, Springer 1998

[D17] The MOSARIM Consortium, ”Estimation of interference risk from incumbent frequency users and services,” Workpackage: General Interference Risk Assessment, www.mosarim.eu, June 2010

9. Abbreviations

ACC	Automatic Cruise Control
BL	Back left
BR	Back right
BSD	Blind Spot Detection
DFT	Discrete Fourier Transformation
EIRP	Equivalent Radiated Isotropic Power
FFT	Fast Fourier Transformation
FMCW	Frequency Modulated Continuous Wave
LCA	Lange Change Assist
LO	Local oscillator
$MG_{S/I}$	Interference Mitigation Gain (also named G_P, but with respect to interference)
NFFT	Number of FFT points
PEC	Perfect Electric Conductor
pol	Polarization
RF	Radio Frequency
SF	Scaling factor for $MG_{S/I}$
HH/hh/pp	horizontally polarized transmit-antenna, horizontally polarized receive antenna
VV/vv/tt	vertically polarized transmit-antenna, vertically polarized receive antenna
HV/hv/pt	vertically polarized transmit-antenna, horizontally polarized receive antenna
VH/vh/tp	horizontally polarized transmit-antenna, vertically polarized receive antenna